Received: 10 January 2024 | Revised: 29 March 2024 | Accepted: 5 May 2024

High Voltage

DOI: 10.1049/hve2.12477

ORIGINAL RESEARCH

Effects of polyurethane hardness on the propagation of acoustic signals from partial discharge

Abdul Samad[1] | W. H. Siew[1] | Martin Given[1] | John Liggat[2] | Igor Timoshkin[1]

[1]Department of Electronic and Electrical Engineering, University of Strathclyde, Glasgow, UK

[2]Department of Pure and Applied Chemistry, University of Strathclyde, Glasgow, UK

Correspondence

Abdul Samad.
Email: abdul.samad@strath.ac.uk

Associate Editor: Fuping Zeng

Abstract

Polymeric insulation is a critical component of high voltage systems. However, exposure to high electric stress can cause partial discharges (PDs) to occur and may result in the deterioration of insulation and lead to dielectric failure. These PD events are accompanied by the production of acoustic pressure impulses in the polymer. Detection of these acoustic pressure impulses can reveal the presence of PDs and locate their source. However, analysing the detected acoustic emission (AE) signal is challenging. The acoustic pressure source's nature and the propagating medium's properties, such as density, viscosity, and elasticity, significantly affect the propagating AE signal. The effects of the hardness of the polyurethane (PU) on the propagating AE signal are reported by the authors based on results obtained from laboratory experiments. It was observed that the decay rate in the magnitude of the acoustic impulse was high in PU at all hardness levels following an exponential behaviour. The analysis of the frequency spectra indicates that the higher frequency components attenuate more strongly with distance. These laboratory results can be valuable for engineers and industries as they provide valuable insight into how the physical characteristics of a material affect the propagation characteristics of AE signals during the detection and location of PD source using the AE detection technique.

1 | INTRODUCTION

As the demand for electrical energy increases, high voltage cables are being used more frequently to transmit more power, and it is crucial to ensure the reliability and economic efficiency of the insulation material used for these cables. Polymeric materials are widely used as insulation for high voltage power cables due to their high dielectric strength, lower cost and ease of processing [1–4]. But these polymeric materials utilised by power utilities are exposed to degradation of their insulation characteristics due to the presence of continuous high electric stress and water [1, 5, 6]. The water from residual moisture, environment and surroundings penetrates the polymer and forms a water tree which, on drying, leaves behind its traces [7]. These channels or tubules provide the conducting path to the electric charges. Over time, this can lead to the initiation of partial discharge (PD) or the formation of electrical trees [8].

Further, the presence of void or roughness of the surface of the insulation during cable manufacturing can result in a highly divergent field in that region, which results in the degradation of the dielectric characteristics of the insulating material, leading to the insulation's breakdown [9–11]. Therefore, to enhance the dielectric strength of polymeric insulating materials, researchers addressed this issue by engineering insulation materials containing nanosized fillers known as 'polymer nanocomposites' [12], but still, there are some fundamental challenges such as the cost of synthesising sufficiently pure materials. Additionally, the nanofillers tend to agglomerate, resulting in non-uniform distribution of nanofillers within the polymer matrix, which can reduce the dielectric strength instead of increasing it [12].

Therefore, to ensure the reliability and continuous electric supply, in parallel with the engineering of novel insulation materials, it is necessary to carry out suitable monitoring techniques to observe the life of the power cables. Many online

and offline PD detection techniques, such as chemical, electrical, and optical, are widely used to detect and locate PD events in various insulating mediums [13]. Chemical detection techniques can only be applied offline, while electrical and optical techniques can be used online to detect PD [13–15]. The disadvantage of the latter two techniques is that the electrical and optical signals are prone to external interference, and the interpretation of the resultant electrical or optical signal becomes very complex [16–18].

The PD events also produce short duration acoustic pulses, which ultrasonic transducers can detect, and the information can be used to locate the source of these PD events [13, 19–21]. This technique is well established in liquid and gas-insulated systems (GIS) to detect the PD and locate its source [22–24], but is still not fully explored in solid insulation systems [18, 25]. Efforts were made to investigate the initiation of PDs due to cavity-type defects in solid insulation materials with regular geometries [26–28]. It was observed that an acoustic signal was emitted, detectable within the audible frequency range. The mechanism behind this acoustic emission was attributed to the vibration of the cavity wall induced by the rapid release of energy during a PD event [21, 26]. A photonic–acoustic technique has been introduced to detect these PD events in polymeric insulation cables [20, 26]. Moreover, if two or more acoustic sensors are used, then the location of the source of the PD signal could be obtained by either the time of arrival (TOA) method or the time difference of arrival (TDOA) method [20, 29].

However, detection of these acoustic emission signals in solid insulation materials is challenging as there are multiple layers of the cable structure which can deteriorate the actual signal [20]. The detection of acoustic emission (AE) signals generated by PDs can be affected by background noise, resulting from electrical interference or mechanical vibrations. As a result, the analysis of the actual AE signal becomes intricate [13, 30]. Moreover, a prominent challenge arises as the AE signal generated by PD experiences attenuation while propagating through polymeric materials [21, 31]. The extent to which the physical characteristics of the material contribute to attenuating the AE signal is unclear as there has been a lack of thorough examinations of this matter. However, understanding the relationship between the physical characteristics of the material and attenuation in propagating acoustic signals is crucial as it defines the propagation capability of the acoustic signal, which is essential for deciding whether to employ this technique for detecting PD in power cable insulation.

Therefore, this study examined the impact of the hardness (one of the physical characteristics) of polyurethane (PU) on the propagation characteristics of AE signals emitted from an electrical discharge used to model a PD event. PU rods with different hardness levels, measured on the Shore scale, namely 40° HSA (soft), 70° HSA (medium), and 90° HSA (hard), were used in this study. The electrical discharge was initiated using needle electrodes near one end of the rod. An acoustic transducer was attached to the other end of the rod to detect the acoustic impulse travelling through the polymeric materials. Overall, the study was aimed to understand how the physical properties of a material, such as its hardness, affect the propagation of acoustic signals and explore the potential of using this information for the detection and monitoring of PD in solid insulating materials.

2 | EXPERIMENTAL

2.1 | Materials

One-metre-long PU rods with varying hardness levels were obtained from the PAR Group Ltd to conduct the study. The PU rods were categorised into three distinct categories based on the Shore scale, namely soft (40° HSA), medium (70° HSA), and hard (90° HSA). The reason for choosing three types of PU materials with different hardness levels was to see the effects of hardness on the propagation characteristics of AE signal, that is, speed of propagation, attenuation in the peak magnitude, and changes in the frequency spectrum of the propagating AE signal with distance. Different rod lengths were cut and the AE signals were observed after their propagation along the rods to allow the influence of propagation distance on the acoustic signals to be determined. The selection of the maximum rod length for each type of PU was based on experimental observations of the detectability of the AE signal. For clarity throughout the study, the PU samples with Shore scale hardness ratings of 40° HSA, 70° HSA, and 90° HSA will be referred to as 'PU40', 'PU70', and 'PU90', respectively. Table 1 shows the length of the sample rods considered to investigate the propagation characteristics for each kind of PU.

2.2 | Experimental setup

A discharge was initiated in the air using a needle–needle electrode topology (stainless steel gramophone needles with a diameter of 1 mm and a tip radius of (5 ± 1) μm) with a 2 mm separation, as shown in Figure 1a. A 3.5 kV (adjustable) DC high voltage source was used to charge a 100 pF capacitor. A 34 MΩ resistor was used to increase the time constant for charging. Once the capacitor was charged, it was isolated from the supply and a second switch was closed to connect the capacitor to the electrodes causing a single discharge event. A Tektronix high voltage probe P6015 A, which has a bandwidth of 75 MHz was used to monitor the voltage across the gap and a high frequency current transformer, HFCT100, (4.8 V/A calibration ratio, 100 kHz–20 MHz 3 dB frequency response,

TABLE 1 The length of samples for various PU specimens.

Material	Length of rod (cm)	Density of the rods (kg/m^3)
PU40	10, 20, 30, 40, 50, 60, 70	1001
PU70	10, 20, 30, 40, 50	1070
PU90	10, 20, 30, 40	1120

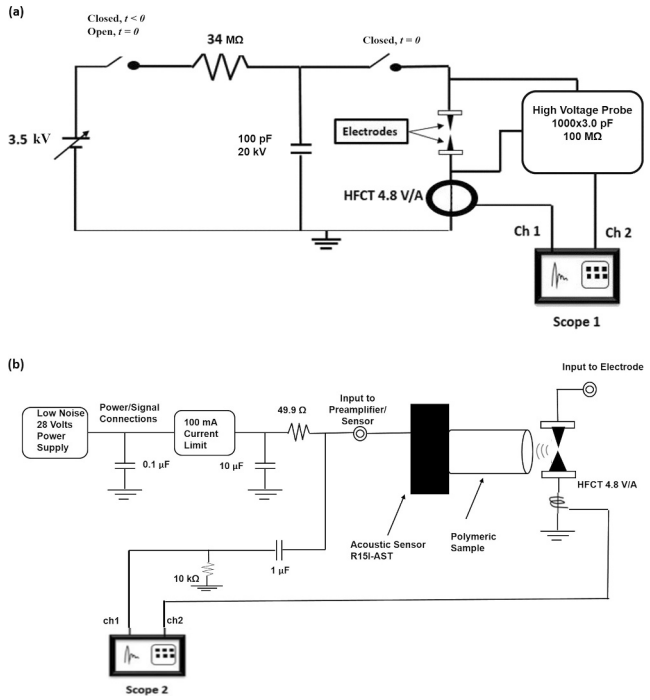

FIGURE 1 Experimental setup to analyse the propagation characteristics of acoustic impulse from PD in PU. (a) Set up to initiate discharge, (b) set up to record the acoustic impulse.

22 ns rise time response) was used to monitor the current in the gap during the discharge event. The signals from these probes were recorded using a Tektronix oscilloscope (TDS2024, 200 MHz, 2 GS/s), referred to as Scope 1.

Figure 1 shows the acoustic measurement arrangements. A R15I-AST 150 kHz, AE acoustic sensor with integral preamplifier (Physical Acoustics, MISTRAS Inc) was used to detect the AE signal. This sensor has a nominal frequency operating range of 50–400 kHz and a resonant frequency of 150 kHz (ref V/µbar) [32]. Figure 1a shows the setup to initiate discharge and subsequent acoustic signal. Figure 1b shows the setup to record the AE signal initiated by a discharge across the electrodes and propagating through the PU rods. The AE signal from the acoustic transducer was fed to Scope 2, (Tektronix oscilloscope, TDS2024, 200 MHz, 2 GS/s) where it was recorded for further analysis. The signal from the HFCT100 was also fed to this scope to allow the triggering of the two scopes to be synchronised. This allowed different timebases to be used on the two scopes, which enabled the capture of the fast transients associated with the electrical signals, which were of the order of 100 ns, while also allowing the propagation time of the acoustic pulse to be considered, which was of the order of 500 µs. In Figure 1a, t denotes time.

The AE signals from the discharge were analysed for each polymeric rod of different lengths. The rod's maximum length was chosen according to the propagation capability of the acoustic pulse in each type of polymer. The 10-cm-long rod was used as a starting point and then the longer rods were used until the AE signal could not be detected.

3 | RESULTS

3.1 | Voltage and current

The capacitor was charged to a voltage of 3.3 kV which was sufficient to cause the gap to breakdown consistently. Figure 2 shows typical voltage and current waveforms for a breakdown event.

3.2 | Detection of AE signals

The propagating AE signals were detected by the acoustic sensor and observed with Scope 2. For each rod length, 20 measurements were taken to ensure that variations in the contact between the sensor and the rod were not affecting the measurements while silicon grease was used as a coupling agent. The sensor was disconnected from the rod then reconnected for each measurement. To convert the detected signal at the sensor into the base unit of pressure, which is the Pascal (Pa), the sensitivity S_{dB} of the sensor, expressed in dB with reference to 1 V/µBar, was first converted to its linear scale equivalent using the formula: Sensitivity (V/µBar) = $10^{S_{dB}/20}$. These values of sensitivity on the linear scale were used to convert the measured voltage signal into pressure (Pa) as: Pressure (Pa) = 0.1·Voltage (V)/Sensitivity (V/µBar). The standard response of the sensor shown in Figure 3 was used to establish a transfer function.

3.2.1 | AE signal propagation in PU40

The propagation capability of an acoustic signal in any material is significantly influenced by the composition, density, and acoustic impedance of the material. Table 1 shows the densities of each polymeric rod used in the study. PU40 has the lowest density among all PU variants used in this study, resulting in lower acoustic impedance compared to other PU variants and potentially higher propagation capability of the acoustic signal in PU40. Figure 4 depicts the AE signals propagating through the PU40 rods of different lengths, with the signal for the 10 cm rod at the top and that for a 70 cm rod at the bottom. AE signals were detectable in PU40 rods up to a length of 70 cm.

3.2.2 | AE signal propagation in PU70

The AE signals propagating through the PU70 rods with various lengths are depicted in Figure 5, with the results for the 10 cm rod displayed at the top and those for a 50 cm rod shown at the bottom. Unlike PU40, where the AE signals were detectable up to 70 cm, the signals in PU70 were only detectable up to 50 cm. This reduced propagation capability of the acoustic signal in PU70 compared to PU40, which can be attributed to the higher density of PU70 and the subsequent increase in acoustic impedance.

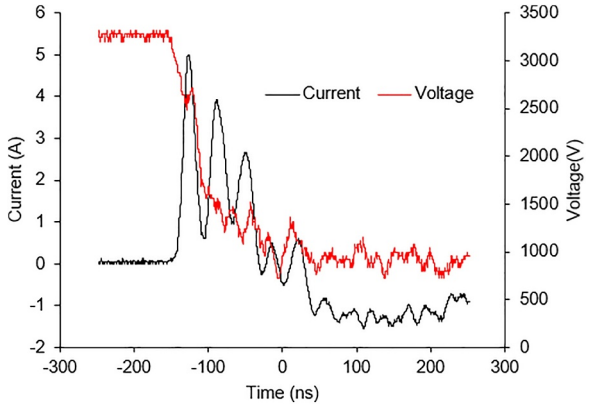

FIGURE 2 Voltage and current impulses across the needle gap.

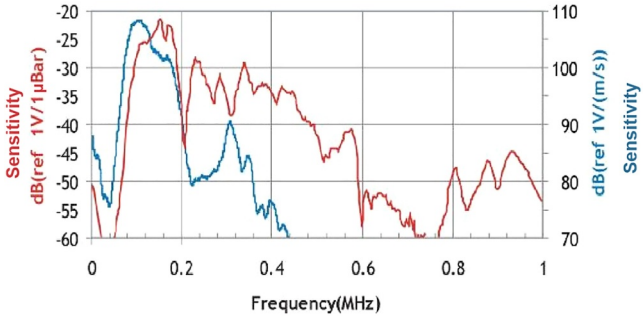

FIGURE 3 The standard response of the R15I-AST acoustic sensor [33].

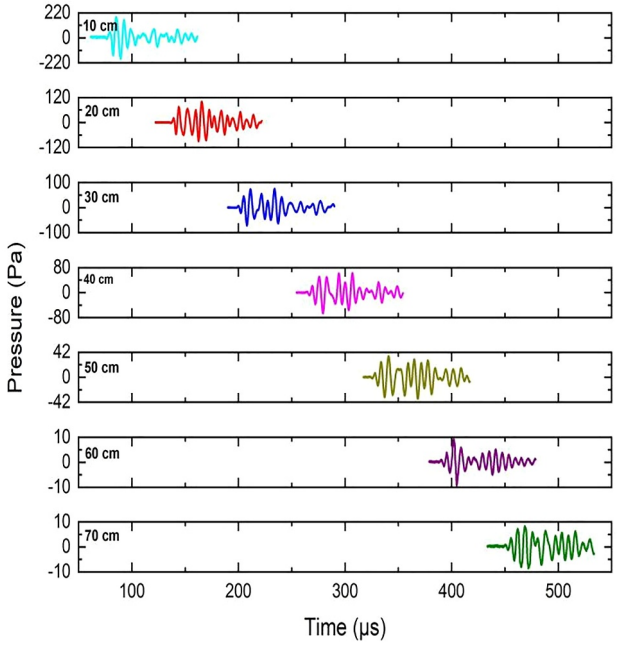

FIGURE 4 Propagation of AE signals in PU40.

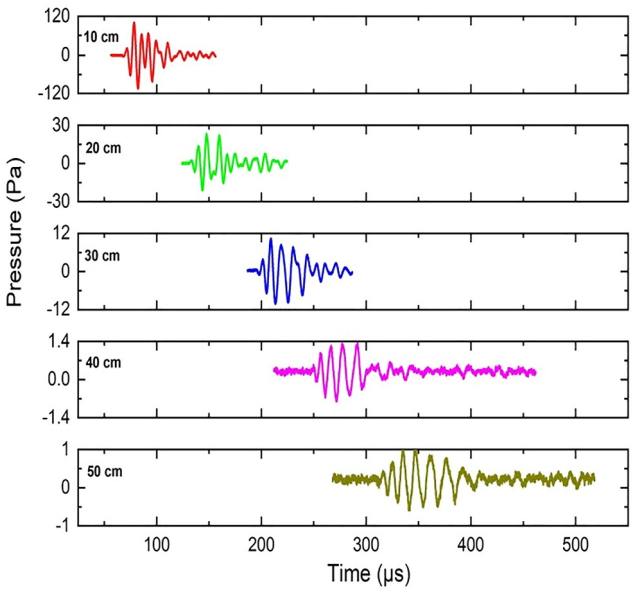

FIGURE 5 Propagation of AE signals in PU70.

3.2.3 | AE signal propagation in PU90

The propagation capability of the acoustic signal was lowest in PU90 among all the PU variants. This can be attributed to the higher density of the material, as evident from Table 1, and the subsequent increase in acoustic impedance offered by PU90. Figure 6 illustrates the AE signals propagating through the PU90 rods with various lengths. The AE signals in the rod were detectable in PU90 up to 40 cm.

3.3 | Drop in peak pressure magnitude of propagating AE signal

To understand the effects of the material's physical characteristics on the propagating acoustic signal, an investigation was conducted to analyse how the peak magnitude of the acoustic signal decreased as the length of the rod increased. The behaviour of the peak magnitude of the acoustic signal in each type of PU is plotted in Figure 7. The magnitude of the peak acoustic signal, $P_{\text{peak}}(x)$ was found to follow an exponential decrease with distance x, that is,

$$P_{\text{peak}}(x) = P_0 e^{-\alpha_p x} \quad (1)$$

where α_p (Np/m) is the attenuation coefficient, x is the distance (the length of the sample), and P_0 is the pressure at the front interface of the sample.

The data in Figure 7 was used to calculate the attenuation coefficient of peak pressure α_p of the acoustic signal as it propagates through the rods by finding the curve of best fit

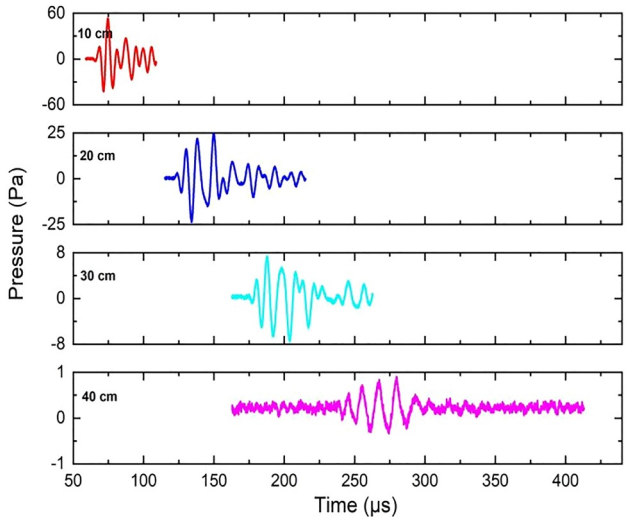

FIGURE 6 Propagation of AE signals in PU90.

accompanied by the 95% confidence interval. This interval provides a measure of the uncertainty associated with our parameter estimation, offering valuable insights into the reliability of our exponential decay behaviour for the given data. Table 2 shows the attenuation coefficient of peak pressure of the propagating acoustic signals in different materials along with the 95% confident intervals and standard error evaluated using the curve fitting tools in MATLAB.

3.4 | Propagation velocity of AE signal in PUs

A tailored adaptation of the time of arrival approach was employed to develop an understanding of the dynamics of acoustic signals and estimate their propagation speed. The moment the scope started recording, the acoustic signal was considered as the arrival time of the acoustic signal. Given that the polymeric rods were positioned at a distance of 3 cm from the discharge source, the acoustic signal was assumed to originate from the discharge, pass through the air, and then transmit through the polymeric rod before being recorded on the scope.

The propagation velocity of the acoustic signal in each material was estimated using the time of arrival of the acoustic signal for the respective lengths of the rods, and a linear fit was made to the time of arrival data, as shown in Figure 8. The boundary between the rod and the air gap is at 0 cm. The fitting curve for each type of polymeric rod can be extrapolated to get the y-intercept. This y-intercept value represents the time for the pressure wave to form in air and for it to propagate across the air gap. Similarly, the gradient $\left(m = \frac{1}{C_{Pu}}\right)$ was used to estimate the propagation velocity (C_{Pu}) of the acoustic signal in each material. The time associated with propagation in the air was calculated as follows: (89.3 ± 0.4), (88.8 ± 0.4) and (89.0 ± 0.4) μs for PU40, PU70, and PU90, respectively. This

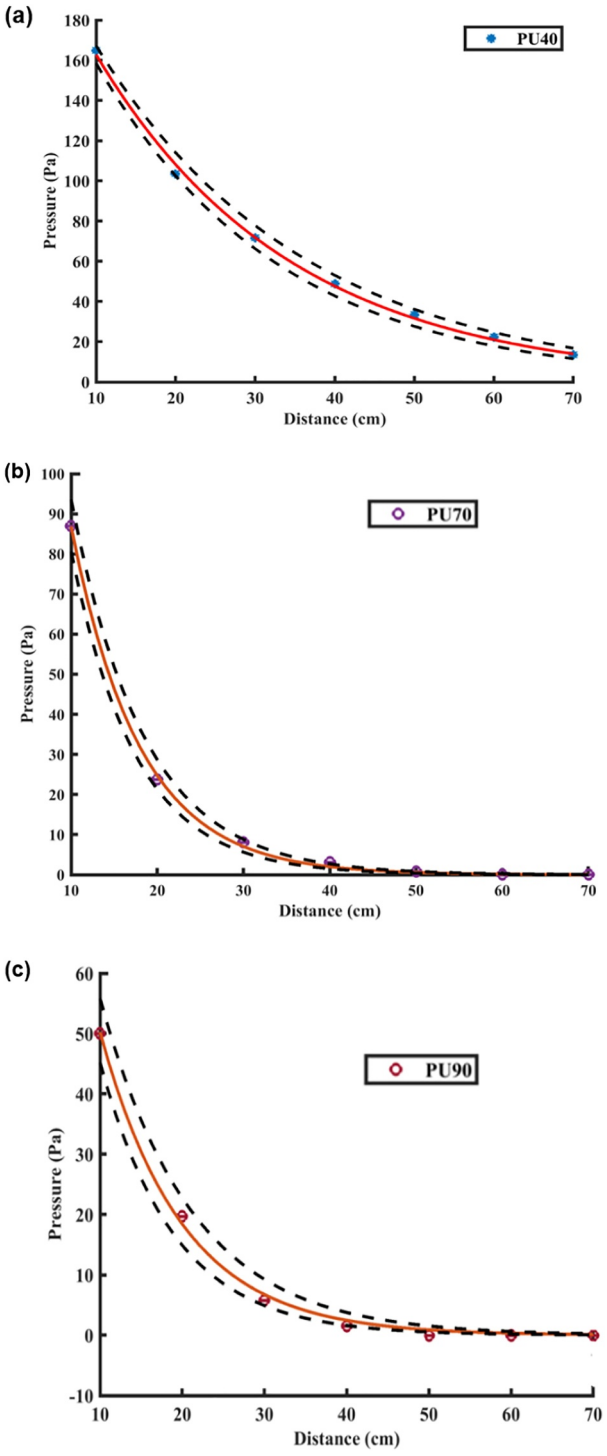

FIGURE 7 Decay in the peak magnitude of the acoustic signal as a function of distance. The plotted points represent the magnitude of the peak acoustic signal at different lengths of the rod along with their 95% confidence intervals (dashed lines), overlaid with the curve of best fit representing the trend in the data. (a) PU40, (b) PU7, and (c) PU90.

suggests that a common value of the speed of sound should be calculated based on the average of these values. This value was 337 ms^{-1}. Table 3 shows the estimated propagation speed in air and the polymeric rods.

TABLE 2 Attenuation coefficient of the peak pressure of the acoustic pulse in polymeric materials. Here, CI-1 represents the 'upper bound' and CI-2 represents the 'lower bound' of the 95% confidence interval.

Material	Peak pressure attenuation coefficient (Np/cm)	Confident interval (CI-1)	Confident interval (CI-2)	Standard error
PU40	0.0409	0.0436	0.0383	0.0014
PU70	0.1258	0.1332	0.1183	0.0038
PU90	0.1004	0.1110	0.0898	0.0054

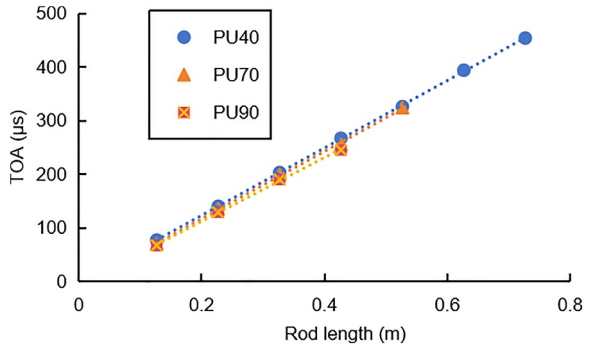

FIGURE 8 TOA of acoustic signal propagating through air and PUs.

TABLE 3 Propagation velocity of acoustic signals in polymeric rods.

Medium	Speed of propagation (m/s)
Air	337
PU40	1589
PU70	1594
PU90	1681

3.5 | Dissipation of energy of the AE signal

The acoustic signal, when propagating through the cylindrical polymeric rods, interacts with the surface of the sensor. The energy associated with this acoustic signal can be determined by integrating the signal's energy over the volume it occupies within the material. Considering the cylindrical shape of the rods and assuming that the pulse travels along the length of the cylinder, we can define two points: x_1 as the point closest to the source of the pressure signal and x_2 as the point farthest from the source. The vector $\overrightarrow{x}_{12}$ points in the direction of signal travel.

Assuming that the pulse can be described at a particular instant of time t_0:

$$P_{t_0}(x) = \begin{cases} 0, & x < x_1 \\ \Phi(x - x_1), & x_1 \le x \le x_2 \\ 0, & x > x_2 \end{cases} \quad (2)$$

where Φ is a function defining the shape of the pressure signal.

The acoustic intensity i, energy per unit volume, at the point x would be defined by the following equation:

$$i(x) = \frac{1}{\rho c^2}(P_{t_0}(x))^2 \quad (3)$$

where ρ represents the density of the cylindrical medium and c is the propagating velocity of the pulse in the cylindrical medium. The energy contained in a volume of the cylinder at position x, can be calculated as follows:

$$\mathrm{d}W = \frac{1}{\rho c^2} A (P_{t_0}(x))^2 \mathrm{d}x \quad (4)$$

Here A represents the surface area of the sensor which is in contact with the cylinder. Therefore, the total energy is given by the following equation:

$$W = \frac{1}{\rho c^2} A \int_{x_1}^{x_2} (P_{t_0}(x))^2 \, \mathrm{d}x \quad (5)$$

By taking into account what is happening in time, then we need to look at the volume swept out, which is associated with our infinitesimal time interval dt. As we can relate time and the position of a point on the signal through velocity, so the integral will become

$$W = \frac{1}{\rho c^2} A \int_{t_1}^{t_2} (P_{x_0}(t))^2 c \, \mathrm{d}t = \frac{1}{\rho c} A \int_{t_1}^{t_2} (P_{t_0}(t))^2 \mathrm{d}t \quad (6)$$

Equation (6) was used to estimate the energy of the acoustic signal detected by the sensor at various points along the rods, using t_1 and t_2 as the leading and trailing ends of the signal in time. The MATLAB 'trapz' function was employed to numerically evaluate the integral. It is important to note that the surface area of the sensor's mating surface was smaller than the surface area of the cylindrical rods, and thus, the variable A represents the surface area of the sensor which was considered while calculating the energy of the signal. While the scalar speeds of propagation of the acoustic signal in each material were used as tabulated in Table 3. The density of each type of PU was also measured in the laboratory and it was found to be 1001, 1070, and 1120 kg/m^3, for PU40, PU70, and PU90, respectively, as displayed in Table 1.

For each length of the polymeric rods, 20 acoustic signals were recorded. The energy of each of these 20 signals was calculated using the above approach and then an average of these 20 signals was calculated. The data were plotted to estimate the attenuation coefficient of energy by finding the curve of best fit accompanied by the 95% confidence interval using the same approach as adopted above while estimating the attenuation coefficient of the peak pressure of the acoustic signal. Table 4 shows the attenuation coefficient of energy of the propagating acoustic signals in different materials along with the 95% confident intervals and standard error evaluated using the curve fitting tools in MATLAB. Figure 9 illustrates the acoustic energy of the signals at various lengths for all types of PUs accompanied by the 95% confidence intervals. Further, the coefficient which describes the dissipation of energy α_E

TABLE 4 Attenuation coefficient of energy of the acoustic signal in polymeric materials accompanied by 95% confidence intervals. Here, CI-1 represents the 'upper bound' and CI-2 represents the 'lower bound' of the 95% confidence interval.

Material	Energy attenuation coefficient (Np/cm)	Confident interval (CI-1)	Confident interval (CI-2)	Standard error
PU40	0.0773	0.0823	0.0723	0.0026
PU70	0.1819	0.1941	0.1696	0.0062
PU90	0.1993	0.2038	0.1949	0.0023

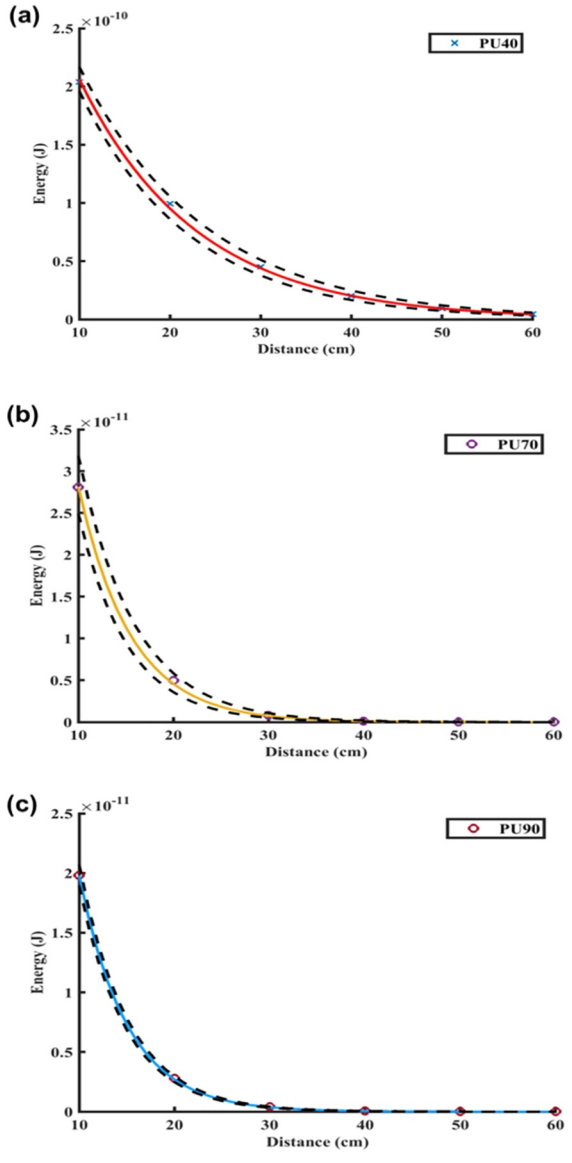

FIGURE 9 Decay in the energy of the acoustic signal as a function of distance. The plotted points represent the energy of the acoustic signal at different lengths of the rod along with their 95% confidence intervals (dashed lines), overlaid with the curve of best fit representing the trend in the data. (a) PU40, (b) PU7, and (c) PU90.

(Np/m) can also be determined based on the calculated energy for rods of different lengths using the following equation:

$$\alpha_E = \left(\ln\left(E_1/E_2\right)\right)/\Delta x \tag{7}$$

where E_1 represents the energy of the acoustic signal detected for a rod of length 1 while E_2 is the energy of the acoustic signal detected for a rod of length 2, and Δx is the difference in length of the two rods.

The energy distribution model can be used to estimate how much electrostatic energy is transmitted into the PU rods as an acoustic pressure signal. To calculate the electrical energy stored in the system, we need to determine the capacitance C and voltage at which the air gap breakdown occurs between the needle electrodes. This relationship can be expressed as follows:

$$W_e = \frac{1}{2}CV^2 \tag{8}$$

where W_e represents the electrostatic energy while V represents the voltage developed across the needle–needle electrode gap. During the experiment, a 100 pF capacitor was used, and the breakdown voltage of the air gap between the needle electrodes was recorded at 3.3 kV. The total electrostatic energy available at discharge was calculated to be 5×10^{-4} J. This energy is converted into heat, light, and pressure acoustic signals when the discharge occurs.

Using Equation (1), we can calculate the acoustic energy available at the surface of the rod facing the acoustic emission source. For PU40, PU70, and PU90, the values for acoustic energy (W) were 4×10^{-10}, 2×10^{-10}, and 1×10^{-10} J, respectively. These values indicate that only a small amount of energy was transmitted into the PU rods as an acoustic impulse. Further, the results suggest that the energy transmission into the PU rods decreases as the hardness of the material increases.

3.6 | Spectrum analysis of AE signal

The spectrum of the AE signal propagating through PU rods with different levels of hardness was analysed using the fast Fourier transform (FFT). To capture the frequency content of the signals accurately while ensuring that crucial information was preserved, the sampling frequency was defined according to the scope's sampling rate. Although it would have been possible to use either upsampling or downsampling techniques to produce effectively higher or lower sampling rates, it was considered best to use the actual sampling rate to prevent the possibility of introducing artefacts in the frequency spectrum.

Moreover, the actual spectrum (A_S) of the detected AE signal can be represented as follows:

$$A_S = \frac{f_{FFT}}{f_{TF}} \quad (9)$$

where f_{FFT} represents the fast Fourier transform of the time domain signal and f_{TF} represents the transfer function of the sensor. The calibration certificate provided with the sensor was used to derive the sensor's transfer function analytically and this is shown in Figure 10.

3.6.1 | Spectrum of AE signal propagating through PU40

Figure 11 shows the spectrum of the AE signal detected after propagating through PU40 for different rod lengths. The spectrum of the AE signal falls between 60 and 200 kHz. It was observed that the magnitude of the spectrum (represented in arbitrary units a.u.) decreased with distance, as a result of the attenuation that was seen in both the peak pressure in Figure 7 and the energy measurements in Figure 9. The attenuation in the higher frequency range of the spectrum appears to be more pronounced than that at lower frequencies.

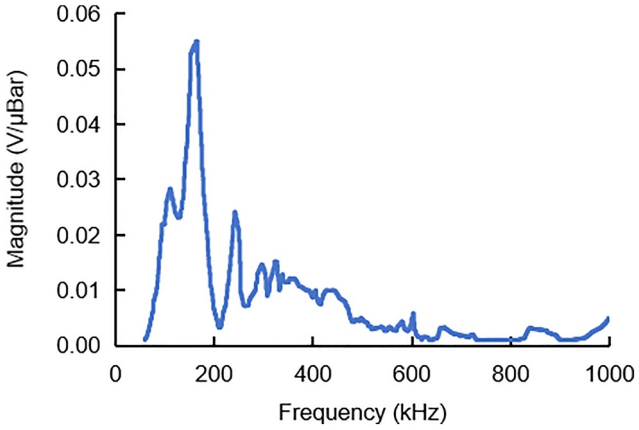

FIGURE 10 The transfer function of the sensor.

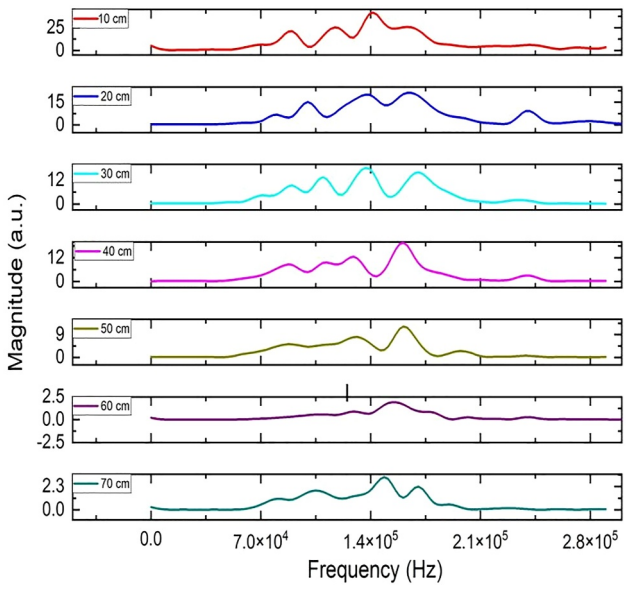

FIGURE 11 The frequency spectrum of the AE signal propagating through PU40 at different lengths.

3.6.2 | Spectrum of AE signal propagating through PU70

Figure 12 shows the spectrum of the AE signal detected after propagating through PU70 for different rod lengths. The signal's frequency range lies between 60 and 170 kHz, and its spectral magnitude decreases with distance as would be expected from the attenuation behaviour observed for pressure in Figure 7 and energy in Figure 9. Furthermore, it was observed that the signal's higher frequency components experienced more damping than the lower frequency components, and this effect was more pronounced than in the case of PU40.

3.6.3 | Spectrum of AE signal propagating through PU90

Figure 13 shows the actual spectrum of the AE signal as it propagates through PU90 for different rod lengths. The signal's frequency range was between 60 and 200 kHz, and its spectral magnitude decreased more rapidly with distance than that in PU40 and PU70. This indicates that the signal experiences more attenuation as it propagates through PU with a higher hardness level.

4 | DISCUSSION

The peak magnitude of the propagating acoustic signal was estimated for different lengths of rods and resulted in exponential decay in peak pressure of the signal with distance. The

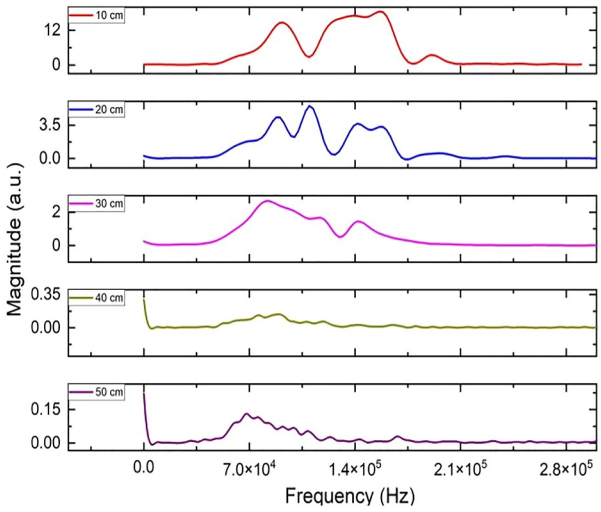

FIGURE 12 The frequency spectrum of the acoustic signal propagating through PU70 at different lengths.

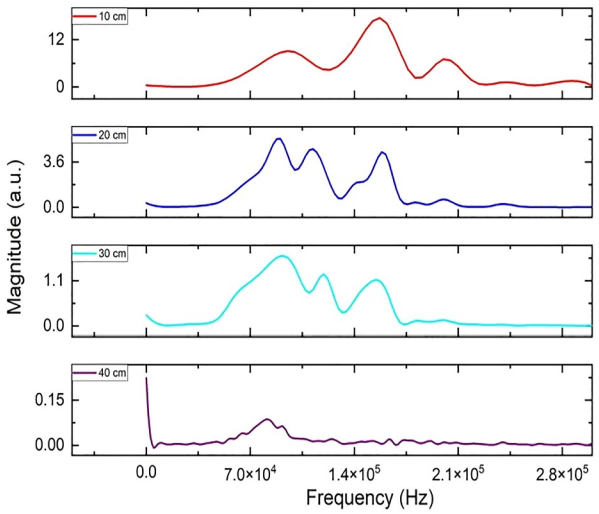

FIGURE 13 The frequency spectrum of the acoustic signal propagating through PU90 at different lengths.

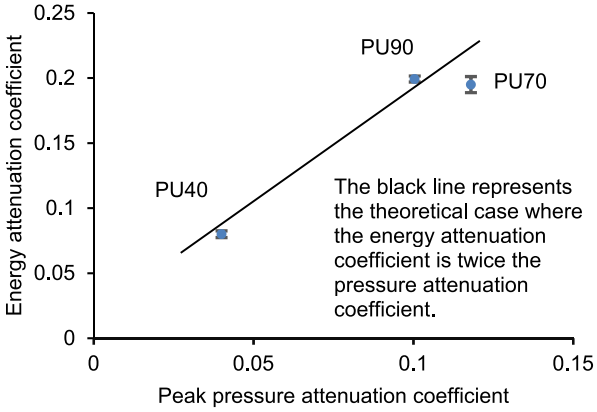

FIGURE 14 Attenuation coefficients of acoustic energy versus peak pressure in PU40, PU70, and PU90.

peak pressure attenuation coefficient of the PU materials increases as the hardness of the material increases as shown in Table 2. However, many of the physical characteristics of PU, for example, the density, will change with the hardness of the material. Therefore, changes in the acoustic properties of the material, such as the acoustic impedance and the speed of propagation may correlate with the hardness but result from these related physical properties. This could also be the case for the observed increase in the propagation velocity of the AE signal as the hardness of the PU increases.

Similarly, the analysis of the attenuation in the energy revealed that the energy of the propagating acoustic signals in PU variants also decays exponentially as shown in Figure 9. Further it was observed that the energy of the acoustic signals attenuates rapidly in PU as the hardness of the material increases as shown in Table 4. Based on Equations (3) and (6), the expected relationship between pressure and the energy of the acoustic signal can be expressed as follows:

$$W(x) \propto (P(x))^2 = P_{02}e^{-2\alpha x} \tag{10}$$

where $W(x)$ represents the energy of the acoustic signal at distance x, while $P(x)$ is the pressure of the acoustic signal at x. Similarly, P_{02} represents the peak acoustic pressure and α is the attenuation coefficient. Therefore, it would be expected that the attenuation coefficient of the energy of the acoustic signal should be twice that of the attenuation coefficient of the acoustic signal's pressure. It was observed that the attenuation coefficients of pressure α_P and the attenuation coefficient of energy α_E for both PU40 and PU90 were in good agreement with Equation (10), but for PU70, the α_E was 7% less than the twice of α_P as shown in Figure 14.

Moreover, the electrostatic energy generated during discharge transforms into heat, light, and a pressure acoustic impulse. This acoustic energy undergoes attenuation as it travels through the air gap between the source and PU rods. Additionally, upon reaching the PU rods, a significant portion of the acoustic impulse is reflected from the rod's surface. The reflection coefficient, influenced by the hardness of the material, is higher for harder PU rods, reducing the energy transmitted into the rod. Consequently, the magnitude of the acoustic impulse in PU is small, primarily attributed to the combined impact of attenuation in the air gap and high reflection at the rod's surface. In practical instances of partial discharge events, where discharges occur within voids or cavities in polymeric insulation, the pressure impulse reflected from the PU rod's surface, which would be lost in air otherwise, becomes available to propagate through the insulation material.

The spectrum analysis of the propagating acoustic signals at different lengths of the rods for each material suggests that the intensity of the higher frequency components of the spectrum was attenuated more strongly than that of the lower frequency components. This is due to crystallinity of the material which causes the scattering of the acoustic signal. As a result, high-frequency components of the signal experience more attenuation than lower-frequency components. Moreover, the distortion can also be attributed to the inherent filtering function of PU materials, wherein variations in the length of the rod and the hardness of PU will lead to alterations in the frequency response of the system. Efforts were undertaken to investigate whether there was any discernible correlation between the magnitude of the frequency components in the spectrum and the length of the rods. However, no consistent correlation was identified. The authors believe that, in addition to observing a single acoustic pulse, there is also a reflection of acoustic wave from the rear of the jig holding the electrodes. This combination of pulses presents problems in identifying an appropriate window for the FFT analysis.

Overall, the results related to the propagation capability of acoustic signals show that the acoustic signals from a discharge have the capability to propagate through the polymeric materials and were detectable for a distance of 70 cm in PU40 rod unlike the observation made in an FEA-based COMSOL simulation model by T. Czaszejko [32]. However, significant differences in the propagation characteristics in polymeric materials used in

this study suggest that each individual of the polymer family reacts differently towards the propagating acoustic signal. Therefore, we cannot rule out the use of acoustic detection techniques to detect and locate PD activity in solid polymeric insulation at short ranges, such as would be found in a cable joint. Similarly, it also suggests that the propagation capability of AE signals significantly depends upon the physical characteristics and morphology of the polymers.

5 | CONCLUSION

This article describes the impact of PU hardness on the propagation characteristics of AE signals generated by electrical discharges. Although both the attenuation coefficients for peak pressure and energy of the acoustic signal showed an exponential decay across all hardness levels of PU, which may limit the utility of acoustic detection techniques in solid insulating materials, it is worth noting that the AE signal remained detectable up to a distance of 70 cm in PU40. This finding suggests that the technique can be effectively applied at cable joints to detect PD despite the attenuation. Furthermore, PU40, characterised by its lower energy attenuation coefficient and flexibility as compared with its counterparts, makes it a promising candidate for use in cable joints where maintaining the integrity of insulation is crucial. However, additional research is required to thoroughly investigate the dielectric properties and the extent of self-healing capabilities within these PU materials. Further studies will help determine the suitability and effectiveness of these materials in cable joint applications and other insulation-related contexts.

CONFLICT OF INTEREST STATEMENT

The authors declare no potential conflicts of interest.

DATA AVAILABILITY STATEMENT

The data that support the findings of this study are available on request from the corresponding author.

ORCID

Abdul Samad https://orcid.org/0009-0000-1700-5017

REFERENCES

1. Su, J., et al.: Electrical tree degradation in high-voltage cable insulation: progress and challenges. High Volt. 5(4), 353–364 (2020)
2. Li, Z., Du, B.: Polymeric insulation for high-voltage dc extruded cables: challenges and development directions. IEEE Electr. Insul. Mag. 34(6), 30–43 (2018)
3. Angalane, S.K., Kasinathan, E.: A review on polymeric insulation for high-voltage application under various stress conditions. Polym. Compos. 43(8), 4803–4834 (2022)
4. Bazli, L., et al.: Electrical properties of polymer blend composites based on silicone rubber/EPDM/clay hybrid for high voltage insulators. J. Composites Comp. 3(6), 18–24 (2021)
5. Li, C., et al.: High temperature insulation materials for DC cable insulation—Part III: degradation and surface breakdown. IEEE Trans. Dielectr. Electr. Insul. 28(1), 240–247 (2021)
6. Saleem, M.Z., Akbar, M.: Review of the performance of high-voltage composite insulators. Polymers 14(3), 431 (2022)
7. Li, Z., et al.: Predicting failure of dynamic subsea cables by electrical insulation breakdown due to water treeing. In: Advances in the Analysis and Design of Marine Structures, pp. 477–484. CRC Press (2023)
8. El-Zein, A., Mohamed, K., Talaat, M.: Water trees in polyethylene insulated power cables: approach to water trees initiation mechanism. Elec. Power Syst. Res. 180, 106158 (2020)
9. Rizwan, M., Chandan, M.R.: Mechanistic insights into the ageing of EPDM micro/hybrid composites for high voltage insulation application. Polym. Degrad. Stabil. 204, 110114 (2022)
10. Ghosh, D., Khastgir, D.: Degradation and stability of polymeric high-voltage insulators and prediction of their service life through environmental and accelerated aging processes. ACS Omega 3(9), 11317–11330 (2018)
11. Arora, R., Mosch, W.: High Voltage Insulation Engineering: Behaviour of Dielectrics; Their Properties and Applications. New Age International (2008)
12. Samad, A., et al.: Structure and breakdown property relationship of polyethylene nanocomposites containing laboratory-synthesized alumina, magnesia and magnesium aluminate nanofillers. J. Phys. Chem. Solid. 120, 140–146 (2018)
13. Refaat, S.S., Shams, M.A.: A review of partial discharge detection, diagnosis techniques in high voltage power cables. In: 2018 IEEE 12th International Conference on Compatibility, Power Electronics and Power Engineering (CPE-POWERENG 2018). IEEE (2018)
14. Refaat, S.S., et al.: A review of partial discharge detection techniques in power transformers. In: 2018 Twentieth International Middle East Power Systems Conference (MEPCON). IEEE (2018)
15. Kumar, A.S., et al.: Online partial discharge detection and location techniques for condition monitoring of power transformers: a review. In: 2008 International Conference on Condition Monitoring and Diagnosis. IEEE (2008)
16. Wu, J., et al.: Measuring method for partial discharges in a high voltage cable system subjected to impulse and superimposed voltage under laboratory conditions. Int. J. Electr. Power Energy Syst. 115, 105489 (2020)
17. Zhang, X., et al.: Review on detection and analysis of partial discharge along power cables. Energies 14(22), 7692 (2021)
18. Govindarajan, S., et al.: A review on partial discharge diagnosis in cables: theory, techniques, and trends. Measurement 216, 112882 (2023)
19. Casals-Torrens, P., González-Parada, A., Bosch-Tous, R.: Online PD detection on high voltage underground power cables by acoustic emission. Procedia Eng. 35, 22–30 (2012)
20. Phung, B., Blackburn, T., Liu, Z.: Acoustic measurements of partial discharge signals. J. Electr. Electron. Eng. Aust. 21(1), 41–47 (2001)
21. Samad, A., et al.: Propagation of acoustic pulse due to PD in polymeric insulating material. In: 2023 INSUCON-14th International Electrical Insulation Conference (INSUCON). IEEE (2023)
22. Sikorski, W., et al.: On-Line partial discharge monitoring system for power transformers based on the simultaneous detection of high frequency, ultra-high frequency, and acoustic emission signals. Energies 13(12), 3271 (2020)
23. Besharatifard, H., et al.: Detection and analysis of partial discharges in oil-immersed power transformers using low-cost acoustic sensors. Appl. Sci. 12(6), 3010 (2022)
24. Lin, Q., et al.: Optimized denoising method for weak acoustic emission signal in partial discharge detection. IEEE Trans. Dielectr. Electr. Insul. 29(4), 1409–1416 (2022)
25. Qin, W.-q., et al.: Distributed detection and acoustic emission waveform retrieval of cable joint partial discharge. IEEE Trans. Power Deliv. 38(4), 2977–2980 (2023)
26. Czaszejko, T., Sookun, J.: Acoustic emission from partial discharges in cable termination. In: Proceedings of 2014 International Symposium on Electrical Insulating Materials. IEEE (2014)
27. Czaszejko, T.: The rustle of electrical trees. In: 2016 IEEE Conference on Electrical Insulation and Dielectric Phenomena (CEIDP). IEEE (2016)
28. Samad, A., et al.: Modelling of propagation characteristics of acoustic pulse from partial discharge in polymeric insulating materials. In: Acoustics. MDPI (2024)

29. Hashim, A.H.M., et al.: Investigation on partial discharge localization in oil based on time of arrival method. In: 2021 IEEE International Conference on the Properties and Applications of Dielectric Materials (ICPADM). IEEE (2021)
30. Ilkhechi, H.D., Samimi, M.H.: Applications of the acoustic method in partial discharge measurement: a review. IEEE Trans. Dielectr. Electr. Insul. 28(1), 42–51 (2021)
31. Stone, G.C.: Partial discharge diagnostics and electrical equipment insulation condition assessment. IEEE Trans. Dielectr. Electr. Insul. 12(5), 891–904 (2005)
32. Czaszejko, T., Sookun, J.: Acoustic emission from partial discharges in solid dielectrics. In: 2014 IEEE Electrical Insulation Conference (EIC). IEEE (2014)
33. Physical Acoustics Mistras' Physicalacoustics /literature/ Sensors/ Model_R15I-AST.Pdf. https://www.physicalacoustics.com/by-product/sensors/R15I-AST-150-kHz-Integral-Preamp-AE-Sensor

How to cite this article: Samad, A., et al.: Effects of polyurethane hardness on the propagation of acoustic signals from partial discharge. High Voltage. 9(5), 1125–1135 (2024). https://doi.org/10.1049/hve2.12477